



**Proceedings of the Sixth International Conference on  
Asian and Pacific Coasts (APAC 2011)**

**December 14 – 16, 2011, Hong Kong, China**

**WAVE-FIELD FLOW STRUCTURES DEVELOPING AROUND  
LARGE-DIAMETER VERTICAL CIRCULAR CYLINDER**

G. ALFONSI, A. LAURIA, L. PRIMAVERA

*Fluid Dynamics Laboratory, Università della Calabria  
Via P. Bucci 42b, 87036 Rende (Cosenza), Italy*

In this work the issue of wave-induced flow structures that develop around a large-diameter surface-piercing vertical circular cylinder is addressed. A strictly-linear wave case is considered and simulated numerically, solving the Euler equations in primitive variables, and the results are compared with those obtained from the corresponding close-form velocity-potential solution. Then, the *swirling-strength* criterion for flow-structure eduction is applied to the primitive-variable Euler-equations-derived velocity field. It is found that differently-shaped flow structures develop at the free surface and under the free surface, in particular at the cylinder wall. This field of structures is not detectable from the potential-derived velocity field, due to the purely mathematical nature of the latter.

**1. Introduction**

In coastal engineering, a widely-used tool for the investigation of wave phenomena is the velocity potential, in which both hypotheses of inviscid fluid and irrotational flow are incorporated. In some cases, a close-form analytical expression of the potential can be devised. In other cases - especially in complex problems of contemporary coastal engineering - no expressions of the potential exist, so that the system of the Euler equations, cast in terms of the potential, can be solved with numerical means, generally with the use of numerical techniques of integral nature. It can be recognized, though, that the assumptions of both inviscid fluid and irrotational flow are rather restrictive, as related to physical phenomena in which real fluids and rotational flows are actually involved. If one wants to give up the hypothesis of irrotational flow, an appropriate strategy for the investigation of wave-related phenomena is represented by the numerical integration of the Euler equations in velocity-pressure formulation. Under this viewpoint it becomes of remarkable importance to investigate the differences that exist between a flow field derived from a velocity potential, and one resulting from the numerical solution of the Euler equation in primitive variables, for the problem at hand. In this work these issues are addressed, with

reference to the case of the diffraction of water waves by large-diameter, surface piercing, vertical circular cylinder. The close form velocity potential for this case is first analyzed (as devised by MacCamy and Fuchs [1]), related to a strictly-linear wave case. Then, the same wave case is simulated numerically, solving the Euler equations in primitive variables. For further investigation of the flow fields, the *swirling-strength* criterion for flow-structure detection (as devised by Zhou, Adrian, Balachandar and Kendall [2]) is applied to the primitive-variable Euler-equations-derived velocity field. It is found that (irrotational) flow structures of tubular type develop at the free surface, and structures with more complex shape develop under the free surface, in particular at the cylinder wall.

## 2. Wave Diffraction and Velocity-Potential Solution

It is well known that, in the case of water waves impinging a vertical circular cylinder, wave diffraction becomes relevant when  $D/L \geq 0.2$  ( $D=2a$  is cylinder diameter  $L$  is wave length), in conjunction with the condition that the value of the Keulegan-Carpenter number  $KC$  at the still-water level be limited as  $KC < 0.44/(D/L)$ . By representing the different wave regimes in graphical form in terms of  $KC$  and  $H/L$  ( $H$  is wave height), the implementation of the above expressions translates in the identification of a zone in which diffraction is increasingly important and the phenomenon is strictly linear (other zones can also be distinguished in which, for example, diffraction is influenced by nonlinear effects, see among others Sarpkaya and Isaacson [3]). As concerns the phenomenon of the diffraction of linear (water) waves by large-diameter, bottom-fixed, surface-piercing vertical circular cylinder, a close form solution in terms of the velocity potential has been devised by MacCamy and Fuchs [1] in terms of Bessel and Hankel functions (see also [3]), as:

$$\varphi = -i \frac{gH}{2\omega} \frac{\cosh[k(z+d)]}{\cosh(kd)} \sum_{p=0}^{\infty} \varepsilon_p i^p \left[ J_p(kr) - \frac{J'_p(ka)}{H_p^{(1)}(ka)} H_p^{(1)}(kr) \right] \cos(p\theta) e^{-i\omega t} \quad (1)$$

( $d$  is still-water level,  $g$  is gravity), where from expression (1) the velocity field ( $u_i = \partial\varphi/\partial x_i$ ) and other relevant quantities can be derived. The maximum nondimensional runup  $R_M^{ND}$  and the maximum nondimensional force  $F_M^{ND}$  on the cylindrical body are given by the following expressions ( $\rho$  is fluid density):

$$R_M^{ND} = \frac{R_M}{H} = \left[ \sum_{p=0}^{\infty} \frac{\varepsilon_p i^p \cos(p\theta_{usp})}{\pi ka H_p^{(1)}(ka)} \right] e^{-i\omega t} \quad (2)$$

$$F_M^{ND} = \frac{F_M}{\rho g H a d} = \frac{2A(ka)}{ka} \frac{\tanh(kd)}{kd} \cos(\omega t - \alpha) \quad (3)$$

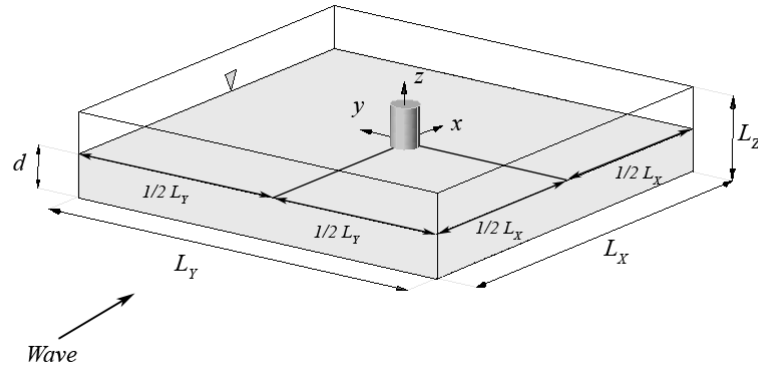


Figure 1. Sketch of the computing domain.

### 3. Numerical Integration of the Primitive-Variable Euler Equations

The system of the Euler equations in velocity-pressure formulation is now considered (the fluid is incompressible and inviscid, the flow is not necessarily irrotational,  $u_i$  is velocity,  $p$  is pressure):

$$\frac{\partial u_i}{\partial t} + u_j \frac{\partial u_i}{\partial x_j} = g\delta_{i3} - \frac{1}{\rho} \frac{\partial p}{\partial x_i} \quad (4)$$

$$\frac{\partial u_i}{\partial x_i} = 0 \quad (5)$$

For the execution of the calculations, the Flow-3D finite-volume computational code has been used. In this code, the free-surface condition is handled with the VOF (volume of fluid) method, that has extensively proven to be able to accurately tracking a wave interface. The meshing technique does not induce mesh distortion during transients (a multi-block meshing technique can be also used to provide higher resolutions in the calculations, where needed). The time-marching procedure includes three main steps: *i*) evaluation of the velocity in each cell using the initial conditions (or previous-time-step values) for the advective pressures (and/or other accelerations), on the basis of appropriate explicit approximations of the governing equations; *ii*) adjustment of the pressure in each cell to satisfy the continuity equation; *iii*) updating of the fluid free surface to give the new fluid configuration based on the volume-of- fluid value in each cell. In the present calculations, the available solution scheme

Table 1a. Wave characteristic parameters.

$D$ (m)	$L$ (m)	$T$ (s)	$H$ (m)	$d$ (m)	$D/L$	$KC$	$ka$	$kd$	$H/L$
12.0	45.1	5.4	2.65	18.0	0.26	0.70	0.84	2.51	0.06

Table 1b. Main computational parameters.

$L_x$ (m)	$L_y$ (m)	$L_z$ (m)	$N_x$	$N_y$	$N_z$	$\Delta x$ (m)	$\Delta y$ (m)	$\Delta z$ (m)	$\Delta t_{tot}$ (s)
90.2	90.2	36.0	450	450	360	0.20	0.20	0.10	54.1

Table 1c. Results.

$R_M^{ND}$	Error rel. to expr. (2)	$F_M^{ND}$	Error rel. to expr. (3)
0.84	-1.40%	2.04	-3.27%

based on the Generalized Minimal Residual (GMRES) method has been used. A specially-assembled computing system has been used for the simulations, that includes 2 Intel Xeon 5660 exa-core multi-core processors (a total of 12 CPUs available), a maximum of 48 GB of RAM, and up to 1.8 TB of mass memory. Boundary conditions of free-slip (and zero wall-normal velocity) have been imposed on the  $x$ - $y$  bottom plane of the computing domain (see at Figure 1), and at the cylinder external surface. On the two  $x$ - $z$  lateral boundary planes and on the  $y$ - $z$  end-plane of the computing domain, outflow conditions have been set, while the free-surface condition holds at the wave surface. On the  $y$ - $z$  inlet plane, the flow field corresponding to an incident linear wave (with the desired characteristic parameters) is generated, and enters the computational domain through the mesh inlet boundary. For the  $(u_i - p)$  Euler-equation simulations, a strictly-linear wave case has been selected, with given characteristic parameters. These parameters are reported in Table 1a, in conjunction with the main computational quantities (Table 1b). In time, the simulations have been run for a total time  $\Delta t_{tot} = 10T$  ( $T$  is wave period). Once the results of the simulations have been obtained, the values of  $R_M^{ND}$  and  $F_M^{ND}$  have been calculated, and compared with those given by expressions (2) and (3), as shown in Table 1c.

#### 4. Flow-Structures Education

Among the existing techniques for vortex eduction, for the scopes of present work, the *swirling-strength* criterion as devised by Zhou, Adrian, Balachandar and Kendall [2] has been adopted (one can refer to Alfonsi [4] for an extensive review of these subjects). By considering the system of the flow governing

equations, an arbitrary point  $O$  can be chosen in the field, and a Taylor-series expansion of each velocity component can be performed in terms of space coordinates with the origin in  $O$ . If  $O$  is located at a critical point, the zero-order terms are zero. From the characteristic equation of the velocity-gradient tensor  $A_{ij}$ , one has:

$$\lambda^3 + P\lambda^2 + Q\lambda + R = 0 \quad (6)$$

where:

$$P = -\text{tr}(A_{ij}); \quad Q = \frac{1}{2} \left\{ [\text{tr}(A_{ij})]^2 - \text{tr}(A_{ij}^2) \right\}; \quad R = -\det(A_{ij}) \quad (7)$$

are the scalar invariants of the velocity-gradient tensor. In the case of incompressible flow,  $P = 0$ , and equation (6) becomes:

$$\lambda^3 + Q\lambda + R = 0 \quad (8)$$

When the discriminant of (8) is positive, the velocity-gradient tensor has one real eigenvalue ( $\lambda_1$ ) and a pair of complex-conjugate eigenvalues ( $\lambda_2, \lambda_3$ ). Zhou *et al.* [2] adopted the criterion of identifying vortices by visualizing isosurfaces of prescribed values of the imaginary part of the complex-eigenvalue pair of the velocity-gradient tensor. One has:

$$\lambda_1 = \lambda_r; \quad \lambda_2 = \lambda_{cr} + i\lambda_{ci}; \quad \lambda_3 = \lambda_{cr} - i\lambda_{ci} \quad (9)$$

The *swirling strength* ( $\lambda_{ci}$ ) represents a measure of the local swirling rate inside a vortical structure, so that isosurfaces of the imaginary part of the complex eigenvalue pair of the velocity-gradient tensor can be used to visualize vortices. The method is general and does not incorporate any restrictive hypotheses. Moreover, the method is frame independent and, due to the fact that the eigenvalue is complex only in regions of local circular or spiralling streamlines, it automatically eliminates regions having vorticity - if any - but no local spiralling motion.

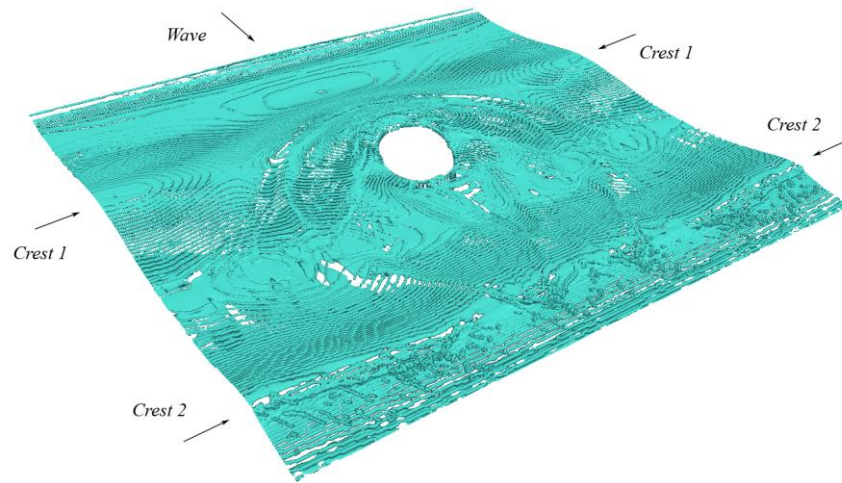


Figure 2. General view of flow structures in the computing domain at  $t = t_{FM}^{Euler}$ .

## 5. Results

Results in terms of flow-structure visualizations are shown in Figures 2/3/4/5 (the threshold value of  $\lambda_{ci}$  used for the visualizations is  $(\lambda_{ci})_{th} = 0.05s^{-1}$ ). In Figure 1 a general view of the full computing domain is given. The flow field is rather regular and substantially symmetric, and exhibits a number of *tubular* (irrotational) structures, concentrated at the free surface. From the distribution of the tubular structures one also obtains a perception of the free-surface configuration in terms of wave crests and troughs, and also of other phenomena, like the accumulation of fluid mass upstream from the cylinder. When the tubular structures are only present at the free surface, other types of structures develop under the surface (arrows 1/2/3 in Figures 3/4/5). The establishment of these structures represents the more relevant difference between the primitive-variable Euler-equations-derived flow field and that derived from the velocity-potential solution, and unveils a physical phenomenon that is impossible to detect from the analysis of the  $\varphi$ -derived field, in virtue of the pure mathematical nature of the latter. Figures 3/4/5 show some close-up views under the free surface and near the cylinder external surface, at  $t = t_{FM}^{Euler}$ . Arrow 1 indicates an (irrotational) flow structure that develops slightly upstream from the cylinder. This structure appears to be the underwater counterpart of the phenomenon of accumulation of fluid mass that verifies - at the surface - upstream from the cylinder, when a wave crest approaches the cylinder. Arrow 2 indicates a flow structure that develops at the cylinder external surface, on the upstream side. This is the most complex and extended structure that has been observed. At

the cylinder basis, a specific substructure develops (arrow 3), that reflects the - inviscid - interaction between fluid, cylinder and bottom wall. This substructure

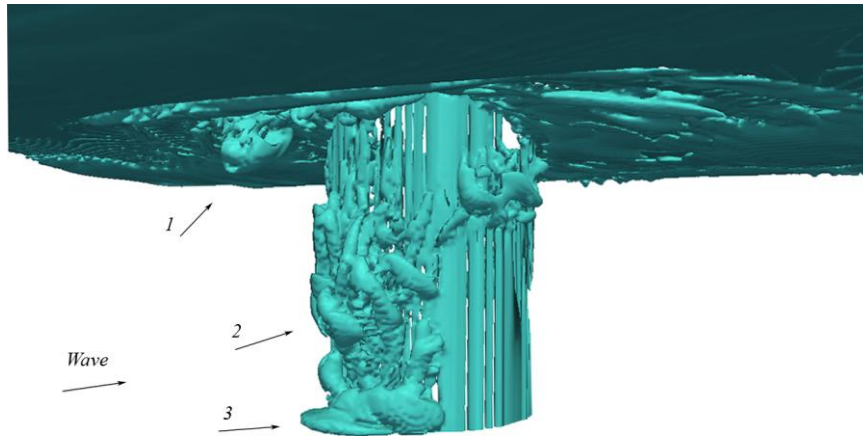


Figure 3. Flow structures at cylinder wall. Front/right view at  $t = t_{FM}^{Euler}$ .

actually represents the inviscid equivalent of the well-known horseshoe vortex that verifies in viscous-fluid flows. Less-extended structures are also present on the cylinder sides (with respect to the upstream-downstream direction).

## 6. Concluding Remarks

In this work, the phenomenon - relatively-well known in the framework of potential-flow theory - of diffraction of water waves caused by large- diameter surface-piercing vertical circular cylinder has been investigated. The study has been performed by integrating numerically the Euler equations in primitive

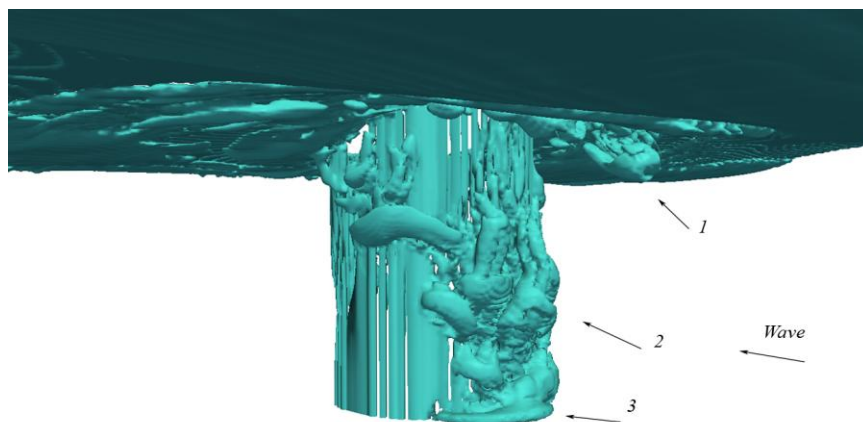


Figure 4. Flow structures at cylinder wall. Front/left view at  $t = t_{FM}^{Euler}$ .

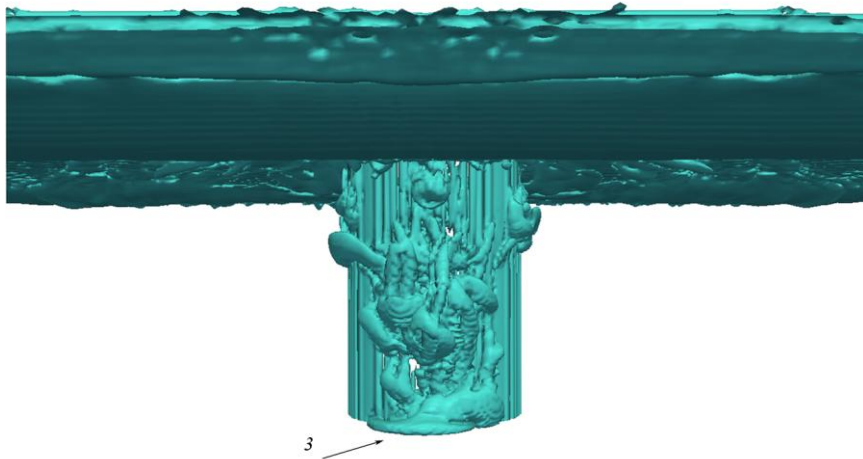


Figure 5. Flow structures at cylinder wall. Front view at  $t = t_{FM}^{Euler}$ .

variables, so that a flow field has been calculated, resulting from the solution of the momentum- and mass-conservation equations. After the application of the *swirling-strength* criterion for flow-structure eduction, differently-shaped structures have been detected in the field. Some of them - of tubular type - are concentrated at the free surface, some others are located under the wave surface, and in particular at the external surface of the cylindrical body. The knowledge of the spatial and temporal behavior of such structures represents a valuable source of information as concerns the development of relevant local effects onto the cylindrical body, caused by the wave motion.

### References

1. R. C. MacCamy and R. A. Fuchs, *Tech. Mem. No. 69*, U.S. Army Corp of Engineers, Beach Erosion Board, Washington, D.C. (1954).
2. J. Zhou, R. J. Adrian, S. Balachandar and T. M. Kendall, *J. Fluid Mech.* **387**, 353 (1999).
3. T. Sarpkaya and M. Isaacson, *Mechanics of wave forces in offshore structures*, Van Nostrand Reinhold, New York (1981).
4. G. Alfonsi, *Appl. Mech. Rev.* **59**, 307 (2006).